Computation of Multipole Moments for Short Thin Wire Chiral Structures

Isak Petrus Theron, David Bruce Davidson and Johannes Hendrik Cloete

Department of Electrical and Electronic Engineering
University of Stellenbosch
Stellenbosch 7600
South Africa

Abstract

This paper considers the computation of the multipole moments of small chiral wire structures. The multipole moments are reviewed and it is shown that the charge induced on the wire must be accurately computed. A quasistatic thin-wire Galerkin Method of Moments formulation has been developed to numerically compute the charge distribution.

The chiral structures under consideration are on the borderline of "thin" and a Body of Revolution Method of Moments formulation has also been developed for use as a check on the accuracy of the thin-wire approximations. It is shown that the "standard" thin-wire formulation is not sufficiently accurate, but the relatively simple addition of an end-cap greatly improves the convergence and accuracy of the formulation with acceptable computation cost.

Finally, the formulation is extended to include bent wires, permitting the electric and magnetic dipole moments as well as the electric quadrupole moment to be calculated for a small chiral structure.

1 Introduction

In 1979, Jaggard et al. [1] initiated the current interest of the electromagnetic engineering community in artificial chiral media at microwave frequencies. They used approximate electric and magnetic dipole moments to analyse a material composed of single turn helixes randomly distributed and oriented in vacuum. Since this work was published, and in particular over the last several years, there has been a substantial amount of research in this field.

In addition to questions regarding the physical realizability of microwave chiral absorbing materials, there are also questions relating to the theoretical basis of the constitutive relations used to date. In [2] Graham, Pierrus and Raab show that when using magnetic dipoles, one needs to include the electric quadrupole term to maintain the origin-independence of the Maxwell equations. In [3] Raab and Cloete show that, for chiral elements much smaller than a wavelength, the optical activity of a chiral medium can be described by the electric quadrupole – magnetic dipole approximation. The theory requires the structures to be much smaller than a wavelength as the scattering from the structures is approximated in terms of only the first three multipole moments. It is also required that the spacing between structures is much less than a wavelength — otherwise the composition will be more of a diffraction grating than a continuum.

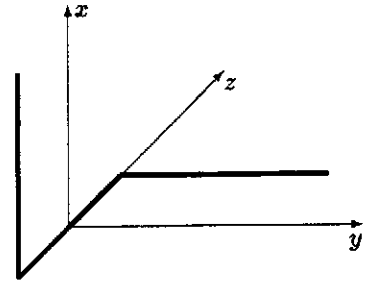

Figure 1: Chiral hook

Construction of a practical medium to validate this theory thus requires chiral structures much smaller than a wavelength. To measure at practical microwave frequencies (eg. 3 GHz) this limits the wire length to a few millimetres, while physical restrictions limit the wire thickness to no less than a few tenths of a millimetre, resulting in "thick" thin wires.

In order to determine the accuracy of the current theoretical models, the contribution of the electric quadrupole term relative to the dipole terms needs to be calculated. This necessitates the calculation of the different multipole moments for a chiral structure. The simplest possible chiral structure, a three dimensional hook as shown in Fig. 1, was chosen such that the calculations — using thin wire approximations — would be as simple

as possible. This structure, at resonance, was also used by Morin for a polarization selective surface [4]. The main advantage of this structure is the ease with which it can be arranged to simulate crystals in the various point groups [5]. This will, however, not be considered in this paper.

To compute the multipole moments, the charges and currents induced on the chiral element are required. Only the simplest structures admit analytical electrodynamic solutions (even the simple half-wave dipole analysis found in most undergraduate electromagnetic textbooks uses an approximation to the current); for an accurate solution of a bent structure such as the chiral hook shown in Fig. 1, numerical methods must be used. The well known method of moments (MoM) will be used in this paper for this purpose. We will show in the next section that a quasi-static formulation suffices for the structures of interest, and that only the induced charge needs to be solved.

Solving for the charge on a quasi-static thin-wire structure appears to be a rather simple problem (it is addressed in many post-graduate texts, for example [6]), but we will show that computing multipole moments requires that the induced charge be very accurately computed. It will be demonstrated that the widely used thin wire approximation must be used with circumspection in this case. Following a brief discussion of the computation of the polarizability tensors, this paper first presents an analysis of a very simple (non-chiral) structure — an electrically short dipole — to test the validity of the techniques. A moderately simple extension to the thin-wire formulation is then used to compute the multipole moments of a chiral structure.

2 The polarizability tensors

In [3] it is shown that the macroscopic electric dipole and quadrupole moments and the magnetic dipole moment are related to the excitation fields and their derivatives via the polarizability tensors

$$\begin{aligned} P_\alpha &= \alpha_{\alpha\beta}E_\beta + \frac{1}{2}a_{\alpha\beta\gamma}\nabla_\gamma E_\beta + \frac{1}{\omega}G'_{\alpha\beta}\dot{B}_\beta + \cdots \\ Q_{\alpha\beta} &= a_{\gamma\alpha\beta}E_\gamma + \cdots \\ M_\alpha &= -\frac{1}{\omega}G'_{\beta\alpha}\dot{E}_\beta + \cdots \end{aligned}$$

from which follow the general form of the constitutive relations for chiral media [3]. In these equations a Greek subscript denotes any of the three Cartesian directions (x, y or z). Repeated subscript notation implies summation over the three components (the Einstein notation) and ∇_β implies the derivative with respect to β. These multipole densities can also be found by spatial averaging of the multipole moments due to the discrete elements. Thus the polarizability tensors describing a composite medium can be calculated from the multipole moments of the inclusions. From [2] the first three multipole moments for a given charge distribution are given by:

$$p_\alpha = \int_v \rho(\boldsymbol{r}) r_\alpha \, dv \tag{1}$$

$$q_{\alpha\beta} = \int_v \rho(\boldsymbol{r}) r_\alpha r_\beta \, dv \tag{2}$$

$$m_\alpha = \tfrac{1}{2}\int_v [\boldsymbol{r} \times \boldsymbol{J}(\boldsymbol{r})]_\alpha \, dv \tag{3}$$

where ρ, $\boldsymbol{J}$ and $\boldsymbol{r}$ have their normal definitions.

As discussed in the introduction, the underlying theory requires the structures to be much smaller than a wavelength. The problem can thus be approached using electroquasistatic approximations [7, Chapter 3] and is formulated as a boundary value problem in terms of the scalar potential, from which the unknown charges can be solved. (Note that the structure is quasi-static and not static, thus the current is non-zero and can be calculated from the spatial integral of the time derivative of the charge.) Since calculating the charges from the current implies a numeric differentiation process, directly solving for the charges will have a distinct advantage. This is the approach adopted here.

Consider the calculation of the dipole moment. It is tempting to view this "observable" as fundamentally similar to the computation of a radiation pattern or a scattering cross-section, typically the type of output required from a full electrodynamic code, since all involve an integration over the current (or charge in the present case). It is widely accepted that the integration process smoothes the effect of errors in the computed current. However, this is *not* so with the dipole moment calculations. The reason is that the integrand in this case involves the *moment* of the charge, that is the charge weighted by the distance from the centre. Hence, errors at the ends of the wire, which are normally insignificant for the typical electrodynamic observables mentioned above, are magnified in this case; furthermore, the charge is singular at the end of a wire, whereas the current is zero.[1]

From this discussion it is obvious that an accurate charge distribution is needed. Before using the thin wire formulation with its desirable properties, the approach must first be carefully validated for this application. This will done using as a test case a single straight wire in a

[1] The electric dipole moment can also be formulated in terms of the integral of the current on the wire, which can be solved dynamically. However, due to the short nature of the wires, significant currents can exist on the end-caps and the axial current cannot be considered to go to zero at the ends of the straight section of wire. The dynamic formulation is thus not a very attractive alternative.

uniform electric field directed along its length, where, as can be seen from Eqs. (1) to (3), only the dipole moment, $\boldsymbol{p}$, is non-zero when referred to the centre of the dipole. There are no exact analytical solutions available for the charge distribution on a thin wire, and an accurate numerical scheme was thus required to provide reference data. Hence a body of revolution method of moments (BOR MoM) formulation was developed, using the Galerkin approach.

3 Body of revolution method of moments solution

The BOR formulation uses entire domain Fourier modes for the circumferential expansion, and conventional subdomain basis functions along the generating curve (also known as the generatrix). Mautz and Harrington's work, along with later extensions, has become one of the standard references for the full electrodynamic BOR MoM formulation [8]. The present quasi-static formulation is similar in concept, although the implementation is of course greatly simplified by the quasi-static nature of the problem.

The subdomain basis functions used were triangular functions along the generatrix (generally referred to as the t direction [8]). This provides a first-order basis function in finite element terminology. Since the electric field is purely z-directed, the charge is independent of ϕ, and hence only the zero-order Fourier mode is needed. The charge may be visualised as being expanded in terms of short cylindrical rings around the z-axis. Reflectional symmetry was also exploited and only one half of the wire was discretised.

Due to the singularity of the charge at the end of the wire, the distribution varies more rapidly towards the end of the wire. Thus it is advisable to use a non-uniform discretisation along the vertical part of the generatrix (the side of the dipole). On the end-cap the discretisation is uniform. The basis functions are shown in Fig. 2. The length of the last segment on the dipole side, b_{ZN}, is set as close as possible to that of the segments on the end-cap, and the segments increase linearly in length towards the centre of the dipole.

The quasistatic MoM formulation is given in Appendix A while Appendix B shows some detail on the evaluation of the integrable singularities which are unavoidable in the BOR MoM formulation.

The resulting charge distribution, for a 3 mm long wire of diameter 0.3 mm in a uniform electric field of 1 V/m directed along its axis, on one half of the wire length, is given in Fig. 3. The dipole moment for this wire was calculated using the charges from the BOR MoM code. Doubling the number of segments resulted in less than 0.01% change in the dipole moment. This result was thus taken to be a good reference value and is used to normalise the dipole moments in Fig. 4.

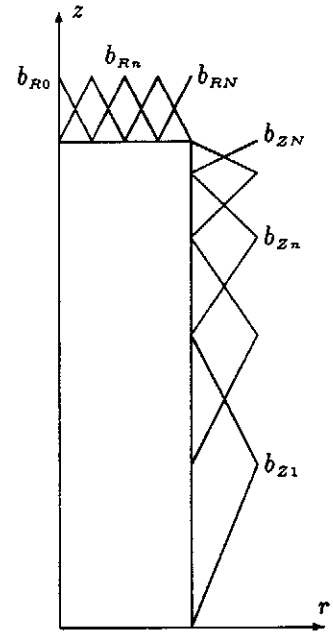

Figure 2: The basis functions on the wire. Note that the whole figure is rotated around the z-axis and is symmetric about the $z = 0$ plane. At the corner, b_{ZN} and b_{RN} are joined to form a single basis function such that continuity of the charge is ensured.

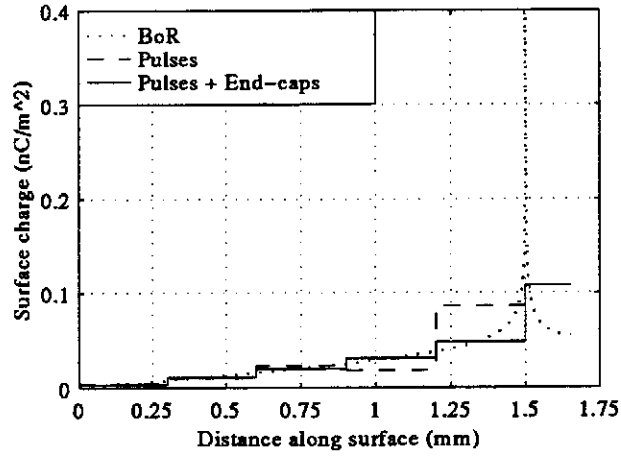

Figure 3: Comparison of the surface charges for the different techniques. The horizontal axis is the t-axis, a length parameter that follows the generatrix. (First it follows the z-axis along the surface of the dipole, then goes inwards along the $-r$ direction on the end-cap.) The 3 mm long wire of diameter 0.3 mm was excited by a uniform field of 1 V/m along its axis.

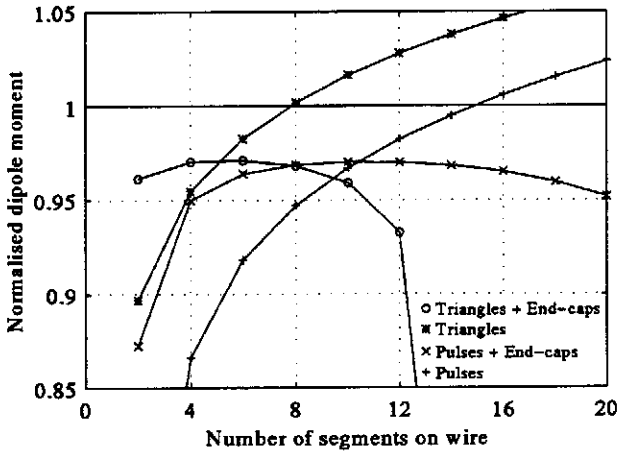

Figure 4: The dipole moments, for a 3 mm long wire with diameter 0.3 mm in a uniform electric field of 1 V/m in the axial direction, plotted against the number of segments. The moments are normalised by $p = 9.305 \times 10^{-20}$ as calculated by the BOR MoM code.

4 The thin wire technique

The electrodynamic solution of thin wires has been extensively studied, initially using analytical techniques (work which reached its peak with the King-Middleton approximate formulas of the 1950's [9]) and more recently using numerical methods, in particular the MoM. The widely used Pocklington formulation is almost 100 years old. Despite the very simple physical structure, sophisticated treatments are required for highly accurate and stable computations. In particular, the following require attention: the end-cap treatment, the source region modelling, and a method for handling thicker wires. All can and have been handled using a BOR MoM formulation, but this a computationally expensive solution, and the BOR MoM formulation is obviously not applicable to bent wires. Janse van Rensburg's doctoral thesis addresses the first two points (end-caps and source region modelling) [10]. Burke and Poggio incorporated an extended thin wire formulation and a simple treatment of wire ends in NEC-2 (this is not a full end-cap treatment) [11, pp. 10-30]; Burke extended this in [12, pp. 28–31]. Popović *et al.* describe a careful treatment of end-caps of flat or hemispherical shape [13, pp. 79–89]. Peterson [14] presents results showing how the careful treatment of end-caps is necessary for a properly converged solution. Fortunately, the source region modelling problem is not a concern with the present scattering formulation.

However, the electroquasistatic solution has received very little attention (certainly in the high-frequency literature). We will now consider the standard thin wire formulation as given by [6, Chapter 12]. A crucial part of the formulation is the reduction of the problem from a two-dimensional surface charge to a one-dimensional line charge. This is known as the thin-wire approximation and has been widely used in powerful numerical electromagnetic codes such as NEC-2. The thin-wire approximation is very attractive, since it removes a dimension from the problem and also avoids the singularity inherent in the formulation. However, the formulation has some restrictions, not least the obvious requirement that the wire indeed be thin!

It is intuitively obvious that for a "thick" wire, the thin wire approximations are invalid; Collin has presented a very elegant discussion of the *theoretical* reasons for the failure of the approximation [15, p. 67–72]. He showed that the high spatial frequency component of the equivalent line current (which the thin-wire MoM codes compute) grows exponentially if the number of harmonics is such that the spatial period becomes less than about πa, where a is the wire radius. Collin's analysis used entire domain basis functions, but similar caveats apply when using subsectional basis functions; it is important to ensure that the discretisation is *coarse* enough to ensure that these harmonics are kept to a minimum. Of course, the discretisation must also be *fine* enough to adequately sample the actual spatial variation of the current (or charge); for sufficiently thin wires, there is a large stable (converged) region between these two requirements, but for thick wires it is possible to move directly from the under-discretised to the over-discretised regimes without the solution evidencing any form of convergence.

Using too fine a discretisation often results in errors around the end points of the wire; the undesirability of this for polarizability calculations is evident from the discussion in section 2. Generally it is accepted that, for the full electrodynamic formulation, the segment length to wire diameter ratio must be greater than two.

The present formulation was implemented with pulse basis and testing functions (i.e. a Galerkin approach) in a similar fashion to that described in [6]. The charge distribution was approximated as a line charge and the potential matched at the outer radius of the wire. (This is the thin-wire approximation already discussed.) The result for the 3 mm wire, shown in Fig. 3, was done with 10 segments on the wire — hence a segment length equal to the wire diameter. It can be seen that there is a considerable error near the end of the wire due to the over discretisation. This error is clearly unacceptable when computing the multipole moments. However, using fewer segments also resulted in large errors, as long segments cannot follow the charge singularity at the end of the wire. The ratio used here seems to be the optimum: half of the normal dynamic requirement that the minimum segment length must be larger than twice the wire diameter.

The dipole moment for the 3 mm wire was calculated using the charges resulting from this formulation. The charges were also calculated using a formulation implementing triangular basis and testing functions. The dipole moments for these two cases are plotted against the number of segments used in Fig. 4. It is clear that although the results throughout the graph are within 15% of the values computed with the BOR MoM formulation the convergence is poor and, without the reference data, one would be hard pressed to decide which discretisation gave the correct result.

Using the charge calculated by the body of revolution code it is found that the end-cap contributes almost 20% towards the dipole moment for the test case. Thus it can be expected that the thin wire technique will give erroneous results, since the end-cap is explicitly excluded from this formulation. An attractive solution to this problem is the inclusion of an end-cap term, and this will be considered in the next section.

5 Thin wire formulation with an added end-cap

The thin-wire technique was expanded by adding one more basis function — a flat disc of constant charge density to model the end-cap.[2] With the axis of the wire in the z-direction and the end-cap located at z', the potential of the end-cap at any position (r, ϕ, z), given by the inner integral in Eq. (7) of Appendix A, is

$$\Phi(\boldsymbol{r}) = \int_0^{2\pi} \int_0^a \frac{r'\, dr'\, d\phi'}{\sqrt{(z-z')^2 + r'^2 + r^2 - 2r'r\cos\phi'}}$$

increasing the complexity of the formulation. One more weighted sample of the field is thus needed. This is obtained by an integral over the end-cap area.

It is important to note that this introduces an asymmetry into the impedance matrix of the moment method formulation.[3] Changing from placing the charge on the axis (and sampling on the surface at the radius) to placing charge at the surface (and sampling on the axis) now results in the transposition of the impedance matrix — with a quite significant effect on the charge distribution. (For the standard straight thin-wire formulation the problem is symmetrical and it is irrelevant whether the charge is viewed as on the surface of the wire and the sampling on the axis or *vice versa*). In accordance with physical principles, the charge is placed on the wire radius and the potential sampled on the axis — thus the outer integral in Eq. (7) of Appendix A reduces to a line integral. Sampling on the axis greatly simplifies the potential of the end-cap to

$$\Phi = 2\pi(\sqrt{a^2 + (z-z')^2} - |z-z'|)$$

where $|z-z'|$ is the distance from the end-cap. Computation of the "self-term" of the end-cap results in similar singularities to those experienced with the "self-term" calculations discussed in Appendix B.

The potential caused by the basis functions on the sides of the wire is reasonably constant on the end-cap, and their contributions are computed by using the value at the centre of the end-cap weighted by its area. (The "self term" is, however, integrated over the full area.) The charge distribution calculated with this technique is also shown in Fig. 3.

The graphs of the dipole moments (Fig. 4) show that incorporating the end-cap does indeed have the desired result of stabilising the convergence — which is now not only stable but also accurate within about 2% of the BOR MoM result. It is interesting to note how neglecting a significant physical feature in the numerical model (the end-cap in the standard thin wire formulation) can impact in unexpected ways, such as in poor convergence. As one would expect, the formulation using pulses converges more slowly than when using triangles.

The most important feature of this graph, however, is that the pulse formulation remains stable for significantly larger number of segments compared to triangular basis functions (up to a segment length equal to wire diameter). The reason for this is presently not clear. Both formulations converge to the same value. Using pulses leads to a much simpler formulation and, even with double the number of segments, shorter computing times than when using triangles. Hence this last formulation — viz. a Galerkin pulse basis function thin wire (with end-cap) MoM approach — was the one finally adopted. The runtime of this technique on a 486 PC was a few minutes compared with a few seconds for the standard thin wire technique (and two hours for the BOR MoM formulation!) For these time scales the added expense of the end-cap is certainly worthwhile, considering the increase in stability, and the computational cost is still much less than that of a full two-dimensional treatment (even one exploiting symmetry).

6 A chiral element

The chiral element is the bent wire shown in Fig. 1. As for the straight wire, sampling for all the wire segments is done on the axis, with the charge placed on the wire

[2] This is only an approximation as the actual charge distribution on the end-cap is much more complicated.

[3] This is due to the fact that the testing and basis functions for the end-cap are the same, whilst for the axial segments, the basis functions lie on the wire surface and the testing functions on the axis. For the end-cap, the equivalent of a line charge would be a point charge at its centre.

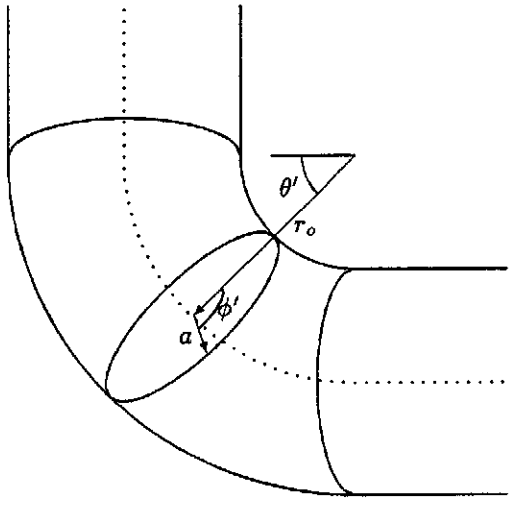

Figure 5: Structure of bend segment.

radius. When sampling on field segments that are not on the same straight section of wire, and are far enough away from the source segments (at least two segments in between them), the source charge was approximated by a line charge on the axis.

The bend requires some special treatment. It is constructed by sweeping the wire cross section along the angle θ' through 90 degrees as shown in Fig. 5, thus joining the two straight wires. The bend is modelled by a single curved segment with the charge placed on the wire surface; this is consistent with the straight segment treatment. When sampling the potential caused by this segment, the integral over the field segment (the outer integral in Eq. (7)) is done analytically,[4] but the source integrand has to be evaluated numerically. Sampling of the field on the bend is done on the axis by numerical integration over θ (measured in the same way as θ').

This treatment of the bend is much more rigorous (and more complex) than merely having a sharp corner. It was implemented to check the effect of the bend and avoid the uncertainty regarding the position of the surface charge in its immediate vicinity. Increasing the radius, r_o, of the curved segment from $r_o = a$, which is as small as the code will allow, to $r_o = 2a$ decreased q_{zz} for a z-directed field[5] by about 3%. Hence it does not appear to have a significant contribution to the calculation of the moments.

The end-cap is treated as a disk for the straight wire section that it terminates; for the other wire sections, it is handled as a point charge on the axis. Treating the end-cap as a point charge removes the expensive calculations necessary when integrating over the endcap without significantly affecting its potential at these wire sections.

As an example, the charge is calculated for the structure in Fig. 1 with 3.12 mm long x- and y-axis legs, 3.14 mm z-axis leg and wire diameter 0.3 mm. The radius of curvature at the two bends in the wire is 1.5 times the wire diameter.[6] The charge distribution for the structure excited by uniform 1 V/m x- and z-directed fields is shown in Fig. 6. Consideration of Fig. 4 led to the conclusion that the optimal segment length is equal to the wire diameter. This required 10 segments on a 3 mm leg. Fig. 6 shows the respective charge distributions calculated with 8 segments on the front leg (27 basis functions including the two bends and the two endcaps[7]) and with 12 segments on the front leg (39 basis functions). It is clear that the charge distribution converged very well. The graphs lie almost on top of each other, with only a small difference near the ends and bends. This is due to the fact that the field is sampled at different points for different segmentations. As one would expect, the E_z-excited charge is anti-symmetrical around the centre of the z-axis. Note also the small peaks at the bends — which is to be expected as a sharp corner would have caused a singularity.

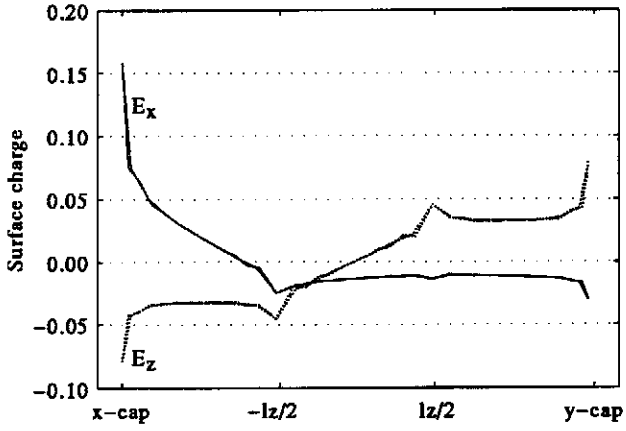

Figure 6: Surface charge in $\mathrm{nC\,m^{-2}}$ for a chiral hook with $l_x = l_y = 3.12$ mm, $l_z = 3.14$ mm, wire radius $a = 0.15$ mm, and $r_o = 1.5\,a$; in an excitation field of 1 V/m using respectively 27 and 39 basis functions. E_x and E_z in the graph indicate direction of the applied electric field.

As the charge distribution is convergent around this point, it was finally calculated using 10 segments on the front leg (33 basis functions in total). This charge distribution was used in Eqs. (1) to (3) to calculate the

[4] Except in the case of the "self-term" or the interaction with the other bend where the field integral is also done numerically — thus requiring three numeric integrations.

[5] This is the moment most sensitive to the radius of the bends.

[6] These dimensions arose from practical considerations in manufacturing an artificial crystalline medium.

[7] The straight part of the z-leg is shorter due to the two bends subtracting from it, and requires one less segment.

	E_x-excitation	E_z-excitation
p_x	2.12×10^{-19}	-1.81×10^{-19}
p_y	-6.79×10^{-20}	1.81×10^{-19}
p_z	-1.81×10^{-19}	3.88×10^{-19}
$\frac{m_x}{j\omega}$	5.29×10^{-23}	-1.41×10^{-22}
$\frac{m_y}{j\omega}$	-1.66×10^{-22}	1.41×10^{-22}
q_{xx}	5.56×10^{-22}	-4.03×10^{-22}
q_{xz}	-3.33×10^{-22}	2.84×10^{-22}
q_{yy}	-1.54×10^{-22}	4.03×10^{-22}
q_{yz}	-1.07×10^{-22}	2.84×10^{-22}
q_{zz}	6.95×10^{-23}	0

Table 1: Multipole moments for a chiral hook with $l_x = l_y = 3.12$ mm, $l_z = 3.14$ mm, wire radius $a = 0.15$ mm, and $r_o = 1.5a$; in a unity uniform field.

multipole moments shown in Table 1. The current density was found by integrating the charge along the wire and differentiating with respect to time. Note that the time derivative of the electric quadrupole moments are of the same order as the magnetic dipole moments.

Formulating the problem without the end-caps and calculating the moments for the same number of segments as used for Table 1 yielded moments within 1% of the values in the table. However decreasing or increasing the number of segments led to poor convergence similar to that shown in Fig. 4. Note that the dipole moments in Fig. 4 are also almost equal at 10 segments which is the number used here. Hence, the advantage of the end-cap is in stabilising the convergence.

With the multipole moments known, the multipole moment densities and medium parameters can be calculated. An artificial crystalline medium was designed with the lattice and orientation of the structures as shown in Fig. 7. The spacings in the plane of the paper are 6.5 and 8 mm respectively and the disks are repeated in the z-direction at intervals of 9.3 mm.

With a host dielectric constant of 1.09 this resulted in dyadic medium parameters [5]

$$\begin{aligned} \epsilon_{xx} &= 1.01\times10^{-11} = 1.14\,\epsilon_o \\ \epsilon_{zz} &= 1.06\times10^{-11} = 1.20\,\epsilon_o \\ \xi_{xx} &= -\omega\,2.54\times10^{-16} \\ \xi_{zz} &= \omega\,2.55\times10^{-16} \end{aligned}$$

for the anisotropic constitutive relations

$$\begin{aligned} \boldsymbol{D} &= \bar{\epsilon}\cdot\boldsymbol{E} + j\bar{\xi}\cdot\boldsymbol{B} \\ \boldsymbol{H} &= j\bar{\xi}^{\,\mathrm{T}}\cdot\boldsymbol{E} + \mu_o^{-1}\boldsymbol{B}. \end{aligned}$$

These have been rigorously derived [5] and are in the so-called Post–Jaggard form [16].

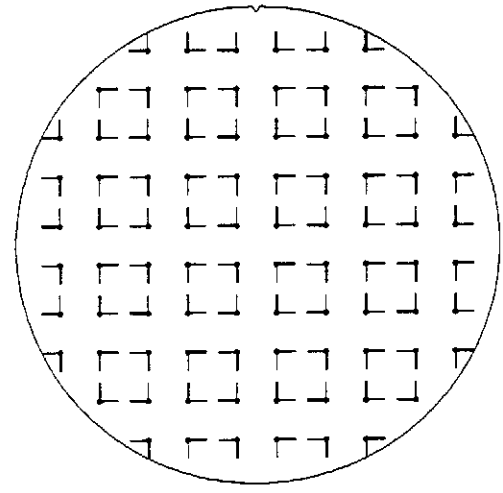

Figure 7: Disklike building element of the crystal. The thick lines are situated in front of the plane of the paper and the thin ones at the back.

At 3 GHz this medium would yield a rotation of 6.5 degrees per metre of the polarization plane of the electric field. The rotation is counter clockwise when viewed in the direction of propagation. The parameters given here were used to predict the rotation inside a waveguide. Agreement of the order of 13% was obtained between predictions and measurements, which is good when considered in the light of probable sources of error [17].

7 Conclusion

This paper has discussed the computation of the multipole moments of an electrically short chiral hook. To obtain the desired result, the charge distribution induced by a uniform electric field was required. It has been obtained via a quasi-static boundary value problem, which was solved using a variety of moment method formulations. A rigorous body of revolution MoM formulation has been presented. Results computed using this BOR MoM code converge rapidly and these computations have been used as a base-line for numerical investigations on thin wire MoM formulations.

The problems arising with the thin-wire formulation for a structure that is on the borderline of "thin" have been discussed. It has been shown that because the observable required from the code is the moment of the charge, the charge must be computed accurately at the ends — precisely where the thin-wire MoM formulations are expected to be least accurate. Results have been presented that show that the conventional thin-wire formulation does not properly converge for these structures. It has been demonstrated that a moderately straightforward extension to the thin-wire approach, viz. adding an

additional basis function to represent the end-cap, gives sufficiently accurate and converged results (within 3% of the BOR MoM result). The code used the same basis and testing functions, i.e. a Galerkin MoM formulation.

The emphasis of this paper has been the accurate computation of multipole moments. These moments can be used to predict medium parameters in the low-frequency regime as briefly described in section 6. The multipole moment calculations are not valid for higher frequencies, but at these frequencies the medium constructed with the chiral elements described here may start behaving more like a diffraction grating than a continuum. The predicted parameters have been experimentally verified.

References

[1] D. L. Jaggard, A. R. Mickelson, and C. H. Papas, "On electromagnetic waves in chiral media," *Applied Physics*, vol. 18, pp. 211–216, 1979.

[2] E. B. Graham, J. Pierrus, and R. E. Raab, "Multipole moments and Maxwell's equations," *J Physics B*, vol. 25, pp. 4673–4684, 1992.

[3] R. E. Raab and J. H. Cloete, "An eigenvalue theory of circular birefringence and dichroism in a non-magnetic chiral medium," *J Electromagnetic Waves and Applications*, vol. 8, no. 8, pp. 1073–1089, 1994.

[4] G. A. Morin, "A new circular polarization selective surface (CPSS)," in *Antenna Applications Symposium*, Univ. of Illinois, Urbana-Champaign, Illinois, Sept. 1989.

[5] I. P. Theron, *The Circular Birefringence of Artificial Chiral Crystals at Microwave Frequencies.* PhD dissertation, University of Stellenbosch, submitted, 1995.

[6] C. A. Balanis, *Advanced Engineering Electromagnetics.* New York: John Wiley and Sons, 1989.

[7] H. A. Haus and J. R. Melcher, *Electromagnetic Fields and Energy.* Englewood Cliffs, New Jersey: Prentice-Hall, 1989.

[8] J. R. Mautz and R. F. Harrrington, "Radiation and scattering from bodies of revolution," *Journal of Applied Scientific Research*, vol. 20, pp. 405–435, June 1969.

[9] R. S. Elliott, *Antenna Theory and Design.* Englewood Cliffs, New Jersey: Prentice-Hall, 1981.

[10] D. J. J. van Rensburg, *On the computation of electromagnetic observables of conducting thin wire radiators.* PhD dissertation, Pretoria University, 1990.

[11] G. J. Burke and A. J. Poggio, "Numerical Electromagnetics Code (NEC) - Method of Moments; Part I: Program Description - Theory," Jan. 1981.

[12] G. J. Burke, "Numerical Electromagnetics Code – NEC-4 – Method of Moments; Part II: Program Description - Theory," Jan. 1992.

[13] B. D. Popović, M. B. Dragović, and A. R. Djordjević, *Analysis and Synthesis of Wire Antennas.* Chichester: Research Studies Press, 1982.

[14] A. F. Peterson, "Difficulties encountered when attempting to validate thin-wire formulations for linear dipole antennas," *Applied Computational Electromagnetics Society Journal,* Special Issue on Electromagnetics Computer Code Validation, pp. 25–40, 1989.

[15] R. E. Collin, *Antennas and Radiowave Propagation.* New York: McGraw-Hill, 1985.

[16] A. Lakhtakia, V. K. Varadan, and V. V. Varadan, *Time-Harmonic Electromagnetic Fields in Chiral Media.* Berlin: Springer-Verlag, 1989.

[17] I. P. Theron and J. H. Cloete, "Microwave optical activity of an artificial non-magnetic uniaxial chiral crystal" and "Waveguide measurement of an artificial uniaxial chiral crystal in the long wavelength regime," in *Chiral'95. International Symposium on Chiral, Bi-isotropic and Bianisotropic Materials*, Pennsylvania State University, 1995.

A Quasistatic MoM formulation

In this appendix we formulate the quasistatic MoM. In the quasistatic formulation the static free-space Green's function is used. Thus the charge is the solution of the integral equation

$$\Phi(\boldsymbol{r}) = \Phi_i(\boldsymbol{r}) + \int_V \frac{\rho(\boldsymbol{r}')}{4\pi\epsilon_o|\boldsymbol{r}-\boldsymbol{r}'|}\,dV' \qquad (4)$$

where $\Phi_i(\boldsymbol{r})$ is the applied potential in the absence of the scatterer and $\Phi(\boldsymbol{r})$ is the boundary value for the potential over a given boundary area. In this paper the applied field is uniform; for example $\Phi_i(\boldsymbol{r}) = -z$ for a z-directed field.

In the method of moments the surface charge distribution, $\rho(\boldsymbol{r})$, is modelled as the sum of a given set of basis functions, $b_n(\boldsymbol{r})$, defined on the surface, S,

$$\rho(\boldsymbol{r}) = \sum_n a_n b_n(\boldsymbol{r}) \qquad (5)$$

with the unknown coefficients, a_n, determining the distribution. The unknown coefficients can be found by

solving Eq. (4) to yield an approximate charge distribution. This is done by multiplying the equation with a number of testing functions $t_i(\boldsymbol{r})$ and integrating over the area S. Using N basis and N testing functions this results in a matrix equation

$$\begin{bmatrix} m_{11} & \cdots & m_{1n} & \cdots & m_{1N} \\ \vdots & & \vdots & & \vdots \\ \vdots & & \vdots & & \vdots \\ m_{i1} & \cdots & m_{in} & \cdots & m_{iN} \\ \vdots & & \vdots & & \vdots \\ m_{N1} & \cdots & m_{Nn} & \cdots & m_{NN} \end{bmatrix} \begin{bmatrix} a_1 \\ \vdots \\ a_n \\ \vdots \\ a_N \end{bmatrix} = \begin{bmatrix} v_1 \\ \vdots \\ \vdots \\ v_i \\ \vdots \\ v_N \end{bmatrix}$$

where

$$v_i = 4\pi\epsilon_o \int_S t_i(\boldsymbol{r}) \left(\Phi(\boldsymbol{r}) - \Phi_i(\boldsymbol{r})\right) da \qquad (6)$$

$$m_{in} = \int_S \int_S \frac{t_i(\boldsymbol{r})\, b_n(\boldsymbol{r}')}{|\boldsymbol{r} - \boldsymbol{r}'|} da'\, da \qquad (7)$$

such that the calculation of m_{in} involves four integrations in total. The inner integral yields the potential due to $b_n(\boldsymbol{r}')$, while the outer integral samples the potential over a given region.

For a conducting body the boundary potential, $\Phi(\boldsymbol{r})$, is a constant. For a thin wire, symmetrical about the origin, $\Phi(\boldsymbol{r}) = 0$ by inspection. In the case of the chiral structure this constant is, however, unknown. As this introduces another variable in the MoM formulation another equation is necessary. This condition is provided for by requiring that the total charge on the wire be zero.

B The BOR MoM formulation

The BOR MoM formulation requires careful attention to certain details and this appendix addresses the computation of the potential and the associated singularity for the self terms of the BOR MoM matrix.

Here these functions are independent of ϕ and can be written as $b_n(z)$ along the dipole side and $b_n(r)$ on the endcap. Because of the non-uniform segmentation, the potential of each basis function must be computed — translational symmetry cannot be used — so it is important to do this efficiently.

The applied potential is required to produce a uniform z-directed field in the absence of the wire thus $\Phi_i(\boldsymbol{r}) = -z$. As the boundary condition the wire surface must be an equipotential surface. With the structure placed symmetrically about the z-axis the boundary potential is zero. Thus the excitation vector is

$$V_i = 4\pi\epsilon_o \int_S b_i(l) z\, da$$

where l is a parameter that can be either z or r depending on where the testing function is located. As discussed earlier, the testing functions are the same as the basis functions and thus denoted $b_i(l)$.

The matrix entry m_{in} for basis functions along the dipole side was determined from the integral

$$\int_S \int_S \frac{b_i(l) b_n(z')\, a\, r}{\sqrt{(z-z')^2 + r^2 + a^2 - 2ra\cos\phi'}} dz'\, d\phi'\, dl\, d\phi$$

where l is as defined before. The inner z' integral was done analytically and the ϕ'-integral numerically. The result is proportional to the potential caused by $b_n(z)$ and is independent of ϕ — thus the outer ϕ integration merely results in multiplication by 2π. The outer l-integration was also done numerically.

The m_{in} entry for the basis functions on the cap was calculated from the integral

$$\int_S \int_S \frac{b_i(l) b_n(r')\, r'\, r}{\sqrt{(z-z')^2 + r^2 + r'^2 - 2rr'\cos\phi'}} dr'\, d\phi'\, dl\, d\phi \qquad (8)$$

where the inner r'-integral was again algebraically evaluated and the ϕ-integral numerically. Here again the outer ϕ integral resulted in multiplication by 2π and the outer l-integration was also done numerically. Note that $z' = \pm L/2$ on the two caps respectively.

In both cases there is a singularity at $\phi' = 0$, when the testing and basis functions coincide (the self-term in MoM parlance). Consider, for example, the inner integral when calculating the self-term for the innermost basis function on the cap — b_{R0} in Fig. 2. If the length of this basis function in the r-direction is d, the basis function can be written as

$$b_{R0}(r) = \frac{d - r}{d}$$

and the inner integral in Eq. (8) becomes

$$\begin{aligned} &\int_0^{2\pi} \int_0^d \frac{(d-r)(d-r')\, r'\, r}{d^2\sqrt{r^2 + r'^2 - 2rr'\cos\phi'}} dr'\, d\phi' \\ &= 2\int_0^{\pi} \int_0^d \frac{(d-r)(d-r')\, r'\, r}{d^2\sqrt{r^2 + r'^2 - 2rr'\cos\phi'}} dr'\, d\phi' \\ &= \frac{r(d-r)}{d^2} \int_0^{\pi} \Big[r(3r\cos\phi' - 2d) \\ &\quad + (d - 3r\cos\phi')\sqrt{d^2 + r^2 - 2dr\cos\phi'} \\ &\quad + r(2r - 2d\cos\phi' - 3r\sin^2\phi') \times \\ &\quad \log\frac{r - r\cos\phi'}{d - r\cos\phi' + \sqrt{d^2 + r^2 - 2dr\cos\phi'}} \Big] d\phi \end{aligned}$$

where the symmetry of the ϕ' dependence is utilised — the integral between 0 and 2π can be written as two times

the integral between 0 and π. It is clear that the third term in the ϕ'-integrand will be singular at $\phi = 0$. This singularity, present at any value of r, can be removed by subtracting a term

$$r(2r - 2d\cos\phi' - 3r\sin^2\phi')\log(1 - \cos\phi')$$

which can be integrated algebraically using[8]

$$\begin{aligned}\int_0^\pi \log(1-\cos\phi)\,d\phi &= -\pi\log 2\\ \int_0^\pi \cos\phi\,\log(1-\cos\phi)\,d\phi &= -\pi\\ \int_0^\pi \sin^2\phi\,\log(1-\cos\phi)\,d\phi &= \tfrac{1}{2}\pi(\tfrac{1}{2}-\log 2)\end{aligned}$$

after expanding the factors. The remaining integrand[9] contains a logarithm that is singular at $r = d$. At this value of r it is simplified to

$$\begin{aligned}&\log\frac{r}{d - r\cos\phi' + \sqrt{d^2 + r^2 - 2dr\cos\phi'}}\\ &= \log\frac{1}{1-\cos\phi' + \sqrt{2(1-\cos\phi')}}\\ &= \log\frac{1+\cos\phi'}{\sin\phi'(\sin\phi' + \sqrt{2(1+\cos\phi')})}\end{aligned}$$

from which the singular $\log\sin\phi'$ can be extracted and integrated analytically between $0 < \phi' < \frac{\pi}{2}$. The remaining term is then integrated numerically (also between $0 < \phi' < \frac{\pi}{2}$) and the original integrand integrated numerically between $\frac{\pi}{2} < \phi' < \pi$. The analytic integration requires the further integrals

$$\begin{aligned}\int_0^{\frac{\pi}{2}} \log(\sin\phi)\,d\phi &= -\tfrac{\pi}{2}\log 2\\ \int_0^{\frac{\pi}{2}} \cos\phi\,\log(\sin\phi)\,d\phi &= -1\\ \int_0^{\frac{\pi}{2}} \sin^2\phi\,\log(\sin\phi)\,d\phi &= \tfrac{\pi}{8}(1-\log 4).\end{aligned}$$

This process unfortunately leads to the subtraction of a large component due to the analytic integration of the singularity from an almost equally large component due to the remaining numeric integral. Thus a few significant digits are lost and the numeric integration has to be done to a very high degree of accuracy. This problem was overcome by dividing the singular component by π, the integration interval, and subtracting it as a constant from the integrand. Thus the two numbers are subtracted before the approximation caused by the numerical integration, requiring much less severe restrictions on the accuracy of the numerical integration to achieve the same final accuracy. The self-terms for the other segments result in similar singularities, which can be subtracted in a similar fashion.

Numeric integration was done with Simpson's rule and halving the interval each time until the results had converged to within 10^{-3} of the last result. The convergence requirements for the inner integral had to be stricter than for the outer integral to converge properly, and 10^{-4} was chosen. The charge on the test case wire was calculated by this technique using 40 segments on the cap and 44 along the axis. About four decimals of accuracy were used in the numerical integrations and the condition number of the MoM matrix was sufficient to preserve this accuracy when inverting the matrix.

[8] Calculated with *Mathematica 2.0*.

[9] Note that $\log a + \log b = \log ab$.

The authors

Isak Petrus Theron was born in 1967 and grew up in Upington, South Africa. He received the B.Eng. and M.Eng. degrees from the University of Stellenbosch in 1989 and 1991 respectively, both cum laude. He is presently a research student in the electromagnetics group at the Department of Electrical and Electronic Engineering at that university. His research is currently directed at modelling anisotropic chiral media by combining optical theories of matter from molecular physics with the analytical, numerical and experimental techniques of classical electromagnetics.

David Bruce Davidson was born in London, England in 1961. He grew up in South Africa. He received the B.Eng., B.Eng. (Honours) and M.Eng. degrees (all cum laude) from the University of Pretoria in 1982, 1983 and 1986 respectively, and in 1991 he received the Ph.D. degree from the University of Stellenbosch. David is presently an Associate Professor of Electrical and Electronic Engineering at the University of Stellenbosch, where he started teaching in 1988 following three years as a research engineer at the national research laboratories. His research interests centre around computational electromagnetics — theory, code development and applications.

Johannes Hendrik Cloete was born in Clocolan, Orange Free State, South Africa in 1945. He received the B.Eng. and Ph.D. (Eng) degrees in Electrical Engineering from the University of Stellenbosch and the MS. degree in Electrical Engineering from the University of California, Berkeley. He has been a professor in the Department of Electrical and Electronic Engineering at the University of Stellenbosch since 1984. His research interests are the electromagnetic properties of microwave materials, experimental methods for characterising them, and antenna engineering.